Palaeogeography, Palaeoclimatology, Palaeoecology xxx (xxxx) 110390

Contents lists available at ScienceDirect

Palaeogeography, Palaeoclimatology, Palaeoecology

journal homepage: www.elsevier.com/locate/palaeo

Centennial- to millennial-scale Asian summer monsoon changes during the MIS 5/4 transition revealed by high-resolution stalagmite records from southwestern China

Rui Zhang[a], Xunlin Yang[a, b, *], Haiwei Zhang[c], Riping Zhang[a], Yingran Yan[a], Saisi Zuli[a], Yong Wang[a]

[a] Chongqing Jinfo Mountain Karst Ecosystem National Observation and Research Station, School of Geographical Sciences, Southwest University, Chongqing 400715, China
[b] Chongqing Key Laboratory of Karst Environment, Southwest University, Chongqing 400715, China
[c] Institute of Global Environmental Change, Xi'an Jiaotong University, Xi'an 710054, China

ARTICLE INFO

Editor: Paul Hesse

Keywords:
Decoupling
Chinese Interstadial 18
Abrupt climatic events
Teleconnection
Yangkou Cave

ABSTRACT

During the Marine Isotope Stage (MIS) 5/4 transition, the global climate changed from an interglacial to a glacial state, and hence it was characterized by high-amplitude climate changes. High-resolution stalagmite records can potentially improve our understanding of climate change during this transition. Here we use a high-precision ^{230}Th-dated, 50-yr-resolution stalagmite δ^{18}O record from Yangkou Cave, in Chongqing, southwestern China, to reveal centennial- to millennial-scale changes in Asian summer monsoon (ASM) intensity during the interval of 98.8–59.3 kyr B.P. (thousands of years before 1950 CE). The record reveals five Chinese Interstadial events, namely CIS 18–22, and pronounced centennial-scale oscillations are evident and verified within these millennial-scale events. There are four centennial-scale events of monsoon strengthening in both CIS 21 and CIS 22, corresponding to Greenland Interstadial events GI 21 and GI 22. By contrast, CIS 18, CIS 19 and CIS 20 differ in both structure and onset time relative to the corresponding GI events during MIS 4. During MIS 5, reduced ice sheet and sea-ice cover and strong Atlantic Meridional Overturning Circulation (AMOC) forced the Intertropical Convergence Zone (ITCZ) towards its northern limit, which enhanced the teleconnection between the ASM and climate change in northern high latitudes. During MIS 5, the millennial-scale events (CIS 21 and 22) show a rapid atmospheric teleconnection between the ASM and the climate of northern high latitudes, but this coupling did not exist during MIS 4. The weakening of Northern Hemisphere summer insolation, the expansion of ice sheets and sea ice, combined with the increased influence of Antarctica, may have led to the decoupling of the Asian summer monsoon and climate change in high northern latitudes.

1. Introduction

Climate change during the Last Glacial Period is characterized by a series of millennial-scale abrupt climatic events, including Dansgaard-Oeschger events (D/O) and Heinrich events (H) (Dansgaard et al., 1993; Heinrich, 1988). With the continuing production of high-resolution records from ice cores and stalagmites, increasing attention is being paid to the internal structure of millennial-scale climatic events (NGRIP Members, 2004; Capron et al., 2010a; Capron et al., 2012; Wang et al., 2008; Wang et al., 2001). Rasmussen et al. (2014) termed the centennial- to millennial-scale events in Greenland ice cores Greenland Stadials (GS) and Interstadials (GI). Centennial- to millennial-scale events, such as the precursor (PE) and rebound (RE) events of the Asian summer monsoon (ASM), are also receiving increasing attention, which may improve our understanding of the relationship between the ASM and other climatic factors (Cai et al., 2006; Liu et al., 2010; Zhao et al., 2010; Zhou et al., 2014; Zhang et al., 2020).

However, many of the published high-resolution stalagmite records are too short in duration to provide continuous coverage of entire marine isotope stages, especially MIS 5 and MIS 4 (Zhang et al., 2017;

* Corresponding author at: Chongqing Jinfo Mountain Karst Ecosystem National Observation and Research Station, School of Geographical Sciences, Southwest University, Chongqing 400715, China.
E-mail addresses: xlyang@swu.edu.cn (X. Yang), zhanghaiwei@xjtu.edu.cn (H. Zhang).

https://doi.org/10.1016/j.palaeo.2021.110390
Received 27 October 2020; Received in revised form 17 March 2021; Accepted 3 April 2021
0031-0182/

Jiang et al., 2019). During MIS 4, only GI 18, GI 19 and GI 20, and H6, are recorded in Greenland ice cores (NGRIP Members, 2004). The stalagmite records from Wulu Cave and Yongxing Cave in China reveal an obvious difference between the Chinese Interstadial (CIS) 18 event and GI 18, mainly in terms of their relative amplitudes of variation (Chen et al., 2016; Liu and Fang, 2019). Because of the relatively low resolution of the records from Sanbao Cave (Wang et al., 2008) and Hulu Cave (Wang et al., 2001), there is no obvious evidence for CIS 18, and in stalagmite JFYK7 from Yangkou Cave, there is a depositional hiatus during CIS 18 (Zhang et al., 2017). The CIS 19 and CIS 20 have long been controversial due to the lack of high-resolution records of the ASM (Cheng et al., 2006; Cai et al., 2015; Zhang et al., 2017; Liu and Fang, 2019). During the MIS 5b/5a and MIS 5a/4 transitions, CIS 21 and CIS 22 are key events for evaluating the evolution of the ASM (Cheng et al., 2016). However, due to the lack of continuous, high-resolution stalagmite records, the focus of attention has been on the age calibration of the MIS 5a/4 boundary, and discussion of CIS 21 and CIS 22 is limited (Zhang et al., 2017; Jiang et al., 2019; Zhang et al., 2020). In addition, while changes in the circulation of the North Atlantic during the MIS 5a/4 transition have been studied (Piotrowski et al., 2005; Guihou et al., 2011; Thornalley et al., 2013), changes in atmospheric circulation (such as the ASM) are less well documented and it is debated whether there was a change in the mechanism driving the ASM (An et al., 2011; Chen et al., 2016; Cheng et al., 2016). Thus there is an obvious need for a greater number of continuous, high-resolution paleoclimatic records from monsoonal Asia in order to address these issues.

Here we report a new high-resolution stalagmite record (JFYK2) from Chongqing, southwestern China, which continuously recorded the evolution of the ASM and most of the centennial- to millennial-scale events during the interval from MIS 5b to MIS 4. Our specific aims are: 1) to investigate the characteristics of centennial- to millennial-scale climatic events during the interglacial/glacial transition from MIS 5 to MIS 4, and 2) to determine the forcing mechanism of the ASM during the interglacial/glacial stages.

2. Site, materials, and methods

Yangkou Cave is located in Jinfo Mountain (28°50′-29°20′ N, 107°-107°20′ E, 2000 m above sea level), Chongqing City, southwestern China (Fig. 1). The study area is located in the eastern part of the Sichuan Basin, to the north of the Yun-Gui Plateau. The climate of the area is dominated by the Asian monsoon system. The ASM system includes two interacting subsystems: the East Asian summer monsoon (EASM) and the Indian summer monsoon (ISM) (Wang et al., 2017; Zhang et al., 2019a, 2019b). The annual mean temperature is 14–21 °C, and the annual precipitation is ~1185 mm (Zhang et al., 2017). The annual precipitation is concentrated from April to October, accounting for 83% of the total, and the relative humidity is above 90% (Chinese Meteorological Administration, http://data.cma.cn).

Stalagmite JFYK2 is 455 mm in length and was collected from the main chamber of Yangkou Cave (29°02′N, 107°11′ E, 2140 m above sea level), ~300 m from the entrance (Fig. 1C). The cave is developed in Permian limestone and has a length of 2245 m. The cave is a shaft-like skylight developed along the northeast fissures, and is classified as a semi-closed cave. The plane form of the cave is a single corridor, with the top being a thin rock layer, and the spatial structure of the cave system is relatively simple. When cut in half and polished, the longitudinal section of JFYK2 is dark brown, with clear growth layers. A hiatus was found at the depth of 30 mm, corresponding to a colour change from dark brown to yellow (Fig. 2A).

Subsamples for ^{230}Th dating were obtained using a 0.9-mm dental drill, and the weight of each subsample was 15–30 mg. Geochronological analyses were performed using a Thermo-Finnigan Neptune Plus, which is a multi-collector inductively coupled plasma mass spectrometer (MC-ICP-MS). The uncertainty of the ^{230}Th dates was calculated as 2σ relative to 1950 CE. The procedures for chemical separation and purification of U and Th are described in Cheng et al. (2013a). The analyses were performed at Xi'an Jiaotong University, China.

For isotopic measurements, a total of 819 subsamples (100 μg) were obtained by drilling along the growth axis of JFYK2, with a diameter of 0.5 mm. Analyses were performed using a Delta V Plus isotope ratio mass spectrometer equipped with a Kiel IV Carbonate Device at the Geochemistry and Isotope Laboratory of Southwest University, China. Results are reported relative to the Vienna Pee Dee Belemnite (VPDB) and standardization was accomplished by using NBS-19 with a $\delta^{18}O$ value of −2.20‰, with the 1-sigma external error of <0.1‰ for $\delta^{18}O$.

3. Results

3.1. Chronology

The dating results for the JFYK2 stalagmite are shown in Table 1. The dating errors are small because the uranium concentrations of the samples are high (~1 ppm), within the range of 100–600 yr. The section from 30 to 455 mm is the focus of the present study (Fig. 2A). An age-depth model was established using Modage software (Hercman and Pawlak, 2012), which shows that the stalagmite was continuously deposited from 98.8 to 59.3 kyr B.P.

3.2. Oxygen isotope record

A total of 819 oxygen isotope data were obtained for the interval of 98.8–59.3 kyr B.P. within stalagmite JFYK2, with the average temporal resolution of ~50 yr. During this interval, the range of variation of $\delta^{18}O$ is −5.5‰ to −10.5‰ , with the average of −7.9‰. During the interval of 98.8–83.9 kyr B.P., the $\delta^{18}O$ values show a gradual depletion, and during the interval of 83.8–76.7 kyr B.P., they show a pronounced depletion, which implies a climatic event, while during 76.8–59.3 kyr B.P., they gradually become enriched. However, these trends are frequently interrupted by intervals of depleted $\delta^{18}O$ values, including during 75.0–72.7 kyr B.P., 72.2–69.0 kyr B.P. and 67.2–63.7 kyr B.P. In addition, there is a significant enrichment trend in $\delta^{18}O$ during 65.3–59.3 kyr B.P., during which the values fluctuate up to −2.5‰ (Fig. 3A).

Before interpreting a stalagmite $\delta^{18}O$ record as a climatic proxy, it is necessary to confirm that the calcite was deposited under isotopic equilibrium fractionation (Hendy, 1971). Hendy (1971) proposed a basis for assessing the isotopic equilibrium fractionation between precipitated calcium carbonate and the parent solution. Based on the rules proposed by Hendy (1971), we drilled out 35 subsamples from five layers, which were subsequently analyzed. As shown in Fig. S1, the range of variation of the $\delta^{18}O$ values within the same stalagmite growth lamina was <0.5‰. Moreover, there is no obvious correlation between the $\delta^{18}O$ and $\delta^{13}C$ values from the central growth axis to the outer edges (Fig. S1), which suggests that stalagmite JFYK2 was precipitated close to isotopic equilibrium conditions and that the $\delta^{18}O$ signal is primarily of climatic origin. A replication test is another robust means for assessing isotopic equilibrium fractionation (Dorale and Liu, 2009). We investigated the $\delta^{18}O$ record of stalagmite JFYK7 from Yangkou Cave, and the results indicated a substantial degree of consistency between this record and that of stalagmite JFYK2 (Zhang et al., 2017) (Fig. 3). In conclusion, both the Hendy's test and the replication test indicate that stalagmite JFYK2 was deposited under conditions close to isotopic equilibrium fractionation, and its $\delta^{18}O$ record primarily reflects climatic changes.

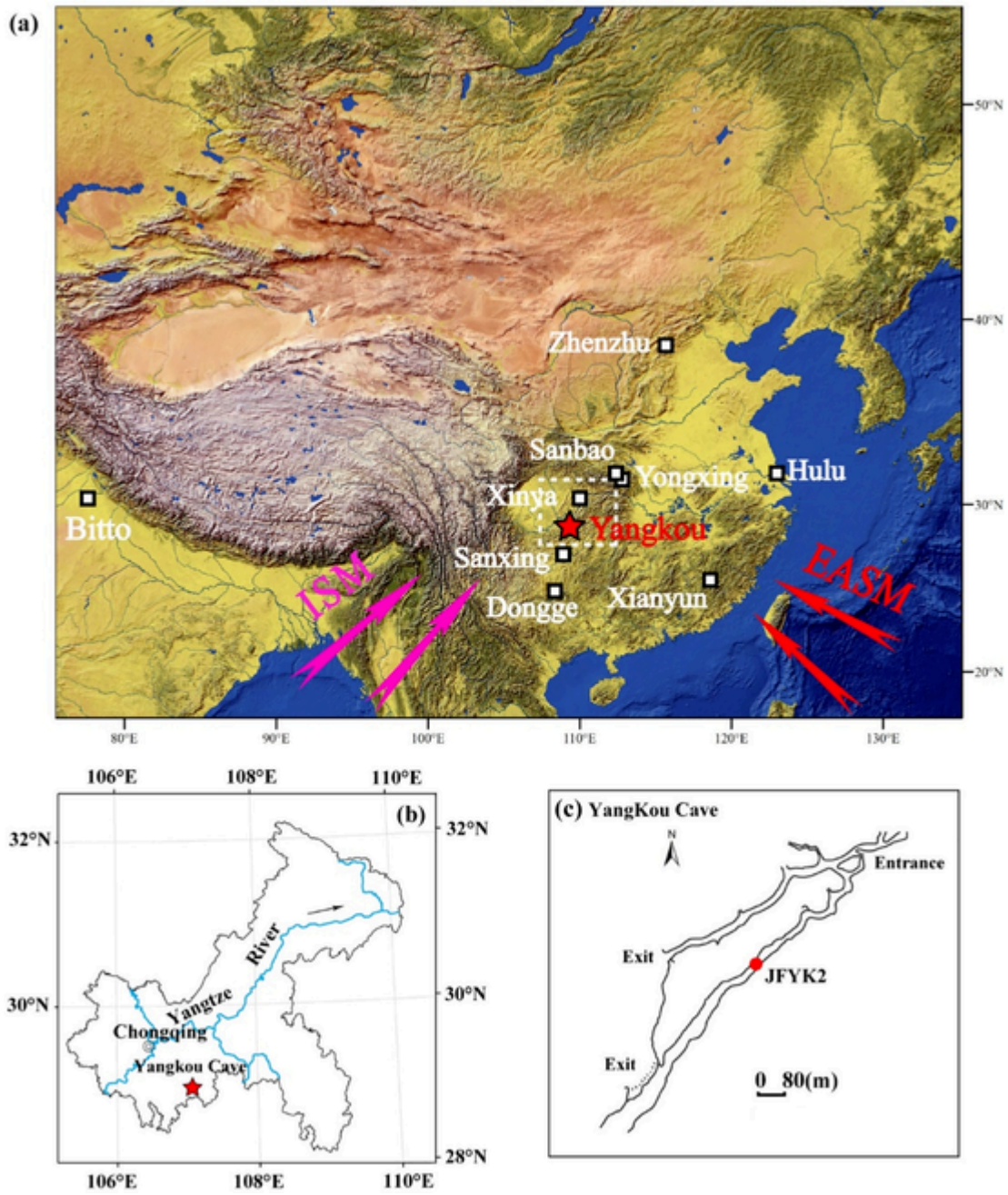

Fig. 1. (a) Topography and atmospheric circulation systems of Asia. Arrows indicate the trajectories of the East Asian summer monsoon (EASM) (red) and the Indian summer monsoon (ISM) (magenta). Also shown are the locations of Yangkou Cave (this study, red star), and Sanxing Cave (Jiang et al., 2018), Yongxing Cave (Chen et al., 2016), Xianyun Cave (Zhang et al., 2020), Zhenzhu Cave (Li et al., 2020), Xinya Cave (Li et al., 2007), Sanbao Cave and Hulu Cave (Wang et al., 2008), Dongge Cave (Cheng et al., 2016), Bitto Cave (Kathayat et al., 2016), (white rectangles). (b) The location of Yangkou Cave (red star) in Chongqing, southwestern China, and Chongqing City (black circle). (c) Sketch map of Yangkou Cave (Chen and Li, 2018), and the red dot indicates the location of sample JFYK2. (For interpretation of the references to colour in this figure legend, the reader is referred to the web version of this article.)

4. Discussion

4.1. Climatic significance of stalagmite $\delta^{18}O$ in monsoonal China

The climatic significance of stalagmite $\delta^{18}O$ in the monsoon region of eastern China remains controversial. For example, there are currently two interpretations of stalagmite $\delta^{18}O$ in the ASM region: 1) stalagmite $\delta^{18}O$ represents the intensity of the ASM/ASM circulation (Cheng et al., 2019; Dong et al., 2015; Wang et al., 2008; Yang et al., 2019a; Yuan et al., 2004), and 2) stalagmite $\delta^{18}O$ is an indicator of local precipitation amount (Zhang et al., 2008). Monitoring studies of Yangkou Cave show that the precipitation $\delta^{18}O$ on the inter-annual timescale can reflect changes in water vapor sources caused by atmospheric circulation (Chen and Li, 2018). Stronger (weaker) ASM circulation results in isotopically depleted (enriched) water vapor via enhanced (reduced) Rayleigh distillation processes (Yuan et al., 2004; Tan, 2014; Yang et al., 2019b). The abrupt climatic events recorded by the stalagmites from Yangkou Cave (Han et al., 2016; Zhang et al., 2017; Du et al., 2019) on the millennial timescale are similar to those recorded by stalagmites from other caves in China since the last glacial period. Based on 16 stalagmite $\delta^{18}O$ records, Yang et al. (2019a) concluded that the $\delta^{18}O$ values of stalagmites track changes in ASM inten-

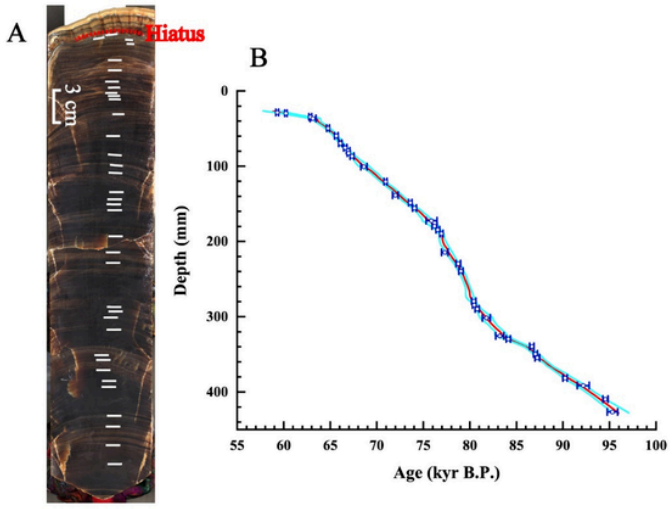

Fig. 2. A. Polished section of stalagmite JFYK2. The white bars are the positions of the U-Th dates used to construct the chronology, and the red dotted line is the position of a hiatus. B. Age model for stalagmite JFYK2, with ^{230}Th dates shown by error bars (2σ) (Hercman and Pawlak, 2012). (For interpretation of the references to colour in this figure legend, the reader is referred to the web version of this article.)

sity across the East Asian monsoon domain, and that they are not solely indicators of precipitation at a particular cave site. Cheng et al. (2019) noted that, overall, precipitation and seasonal precipitation reconstructions do vary across this highly diverse region. As a consequence, we argue that the stalagmite δ^{18}O record of Yangkou Cave is not solely a local precipitation record and that it also provides insights into variations in the intensity of the ASM on a large spatial scale, with depleted δ^{18}O values indicating a strong ASM and enriched values of a weaker ASM, as it has been noted elsewhere (Cheng et al., 2009, 2019; Dong et al., 2015; Wang et al., 2008; Yuan et al., 2004).

4.2. Centennial- to millennial-scale climatic events during MIS 5

The δ^{18}O record of stalagmite JFYK2 reveals two millennial-scale events of monsoon strengthening during MIS 5b-5a (CIS 21 and CIS 22), and they are characterized by a series of centennial-scale oscillations, similar to the changes within millennial-scale events GI 21 and GI 22 recorded in Greenland ice cores (Capron et al., 2010a; Rasmussen et al., 2014) (Fig. 4). In stalagmite JFYK2, the CIS 21 event is interrupted by three short, weak monsoonal events (centered at 81.1 kyr B.P., 78.6 kyr B.P. and 77.2 kyr B.P., respectively) and four centennial-scale strong monsoon events (CIS 21a, CIS 21b, CIS21c and CIS21d). CIS 21a and CIS 21b correspond to GI 21 rebound-events (Capron et al., 2010a; Jiang et al., 2019; Moseley et al., 2020) (Fig. 4B), which may demonstrate that the centennial-scale GI 21 rebound events are widely recorded in stalagmites in the monsoon region of China (Jiang et al., 2019). In the JFYK2 δ^{18}O record, there is a short, weak monsoonal event at 81.1 kyr B.P., with an δ^{18}O enrichment of ~1.5‰. There is also a monsoonal weakening event at 81.1 kyr B.P., recorded by stalagmite δ^{18}O data from Xianyun Cave (XY12) and Zhenzhu Cave (PS1) (Fig. 4C, D). Rasmussen et al. (2014) only divided the GI 21 event into three significant warm events. According to the NGRIP Greenland ice core record, the variation of δ^{18}O at ~82.3 kyr B.P. exceeds 2‰, and there are pronounced differences in the climate of Greenland before and after this cold event. During the CIS 21d event, a series of multi-decadal- to centennial-scale high-frequency fluctuations in the δ^{18}O record of stalagmite JFYK2, correspond to climatic fluctuations during 84.8–82.3 kyr B.P. in the NGRIP ice core δ^{18}O record (Fig. 4). Moreover, differences in the transition of CIS 21d in stalagmite records from monsoonal China may be caused by different water vapor sources (Maher and Thompson, 2012; Clemens et al., 2010). In addition, the abrupt depletion in the stalagmite JFYK2 δ^{18}O record at ~84.4 kyr B.P. possibly corresponds to the CIS 21 precursor event (21-PE) in the East Asian monsoon region (Zhang et al., 2020). This event corresponds well with the GI 21-PE event (Boch et al., 2011; Capron et al., 2010a; Moseley et al., 2020).

During the interval of 91.4–86.8 kyr B.P., there are four strong monsoon events (CIS 22a, 22b, 22c and 22d) within CIS 22 recorded in stalagmite JFYK2, similar to the δ^{18}O record of stalagmite PS1 (Li et al., 2020) (Fig. 4). Overall, therefore, there is a good correspondence between the centennial-scale events within the CIS 22 event recorded by stalagmites in the Asian monsoon region and within the GI 22 event recorded by the NGRIP δ^{18}O record (Rasmussen et al., 2014).

The δ^{18}O record of stalagmite JFYK2 indicates that during MIS 5b and 5a, there was a close relationship between the ASM and temperatures at northern high latitudes on the centennial- to millennial-scale, while the CIS events recorded by stalagmites in the Asian monsoon region corresponded to internal climatic oscillations within the GI events recorded in Greenland ice core. In addition, during MIS 5a, there were numerous significant centennial-scale monsoon events in the ASM region, indicating the climatic instability of the ASM during the MIS 5 interglacial period.

4.3. Centennial- to millennial-scale climatic events in MIS 4

Due to the lack of high resolution and continuous records, the CIS 18 event is not yet clearly defined in stalagmite records from the Asian monsoon region (Wang et al., 2001, 2008; Zhang et al., 2019a). There was no interruption in the growth of stalagmite JFYK2 within CIS 18 and there were nine ^{230}Th age control points, resulting in a temporal resolution of up to 50 yr, making it possible to investigate its fine-scale internal structure and hence the detailed evolution of the Asian summer monsoon at this time.

The duration of CIS 18 in the JFYK2 stalagmite δ^{18}O record is ~3.4 kyr (67.3–63.5 kyr B.P.), indicating the occurrence of three centennial-scale monsoon strengthening events (CIS 18a, 18b and 18c), which depict a stepwise change in the intensity of the Asian summer monsoon within the CIS 18. The basis for subdividing the internal structure of CIS 18 is the occurrence of two weak monsoon events (at 65.5 and 64.5 kyr B.P.), especially the latter which lasted for 300 yr, and these events depict a stepwise change of the Asian summer monsoon intensity during CIS 18 (Li et al., 2007; Chen et al., 2016; Zhang et al., 2017) (Fig. 5). The amplitude of variation of CIS 18a in the stalagmite JFYK2 record is low, but it is higher in Xinya Cave and Yongxing Cave (Li et al., 2007; Chen et al., 2016). Because of a growth interruption in the stalagmite JFYK7 record from Yangkou Cave, only the end of CIS 18a is present (Zhang et al., 2017). CIS 18b (65.4–64.4 kyr B.P.) in the JFYK2 stalagmite record represents a rapid strengthening of the ASM, while in the stalagmite records from Yongxing Cave and Xinya Cave, the fluctuations are minor. In the JFYK2 record, most of the prominent fluctuations in CIS 18c are concentrated within the interval of 67.3–65.4 kyr B.P., with the variation of δ^{18}O being above 2‰, and they lasted for a substantial interval (~2 kyr). In the case of CIS 18c, the JFYK2 and JFYK7 δ^{18}O records are similar (Zhang et al., 2017). The stalagmite record from Yongxing Cave also contains pronounced monsoon strengthening events, during 67.5–65.7 kyr B.P. (Chen et al., 2016). In the stalagmite JFYK2 δ^{18}O record, CIS 18 contrasts sharply with GI 18 in the Greenland ice core record (Capron et al., 2010a; Rasmussen et al., 2014). Based on the NGRIP δ^{18}O record, GI 18 is a brief climatic interval lasting for 200 yr, with minor fluctuations (~8‰) (NGRIP Members, 2004). Stalagmites HÖL18 and KC1 collected from the European Alps provide only an incomplete record of GI 18. According to the stalagmite KC1 δ^{18}O record, there were several small-scale cooling events prior to GI 18, which are also contemporaneous with the mon-

Table 1
Isotopic composition of uranium and thorium and ^{230}Th ages for Yangkou Cave speleothems as determined by MC-ICP-MS.

Sample Number	Depth	^{238}U		^{232}Th		^{230}Th / ^{232}Th		δ^{234}U*		^{230}Th / ^{238}U		^{230}Th age(yr BP)		$\delta^{234}U_{Initial_{**}}$		^{230}Th age(yr BP)	
	(mm)	(ppb)		(ppt)		(atomic*10^{-6})		(measured)		(activity)		uncorrected		corrected		corrected	
JFYK2–1	29	7150.7	±8.2	13,819	±277	4143	±83.1	143.4	±1.4	0.4856	±0.0007	59,489	±151	170	±2	**59,374**	**±155**
JFYK2–2	30	8297.9	±6.2	6006	±120	11,111	±222.8	136.0	±1.2	0.4878	±0.0005	60,392	±129	161	±1	**60,308**	**±130**
JFYK2–3	35	7970.4	±6.4	2973	±60	22,163	±444.7	131.5	±1.3	0.5014	±0.0005	62,997	±141	157	±2	**62,921**	**±141**
JFYK2–4	37	11,099.6	±28.9	1880	±42	48,271	±1074.3	116.5	±2.3	0.4960	±0.0015	63,283	±316	139	±3	**63,213**	**±316**
JFYK2–5	50	15,156.7	±14.3	232	±5	550,569	±12,709.3	129.5	±1.3	0.5117	±0.0006	64,898	±145	156	±2	**64,832**	**±145**
JFYK2–6	60	16,334.1	±23.8	360	±8	393,806	±8582.4	149.4	±1.4	0.5267	±0.0009	65,782	±187	180	±2	**65,714**	**±187**
JFYK2–7	70	12,710.3	±16.8	485	±10	228,380	±4738.8	147.4	±1.4	0.5282	±0.0008	66,213	±177	178	±2	**66,145**	**±177**
JFYK2–8	76	9816.2	±12.3	431	±9	207,946	±4331.9	192.8	±1.4	0.5539	±0.0008	66,738	±175	233	±2	**66,670**	**±175**
JFYK2–9	80	11,628.5	±15.7	512	±10	203,908	±4171.7	169.1	±1.4	0.5441	±0.0009	67,062	±185	204	±2	**66,994**	**±185**
JFYK2–10	83	13,113.8	±12.5	627	±13	187,247	±3866.8	165.7	±1.4	0.5426	±0.0006	67,107	±157	200	±2	**67,040**	**±157**
JFYK2–11	87	12,872.8	±19.0	393	±8	297,751	±6334.3	179.6	±1.5	0.5518	±0.0010	67,477	±204	217	±2	**67,409**	**±204**
JFYK2–12	101	7301.3	±14.9	1832	±44	36,803	±882.6	181.2	±2.3	0.5602	±0.0015	68,750	±323	220	±3	**68,679**	**±323**
JFYK2–13	121	6697.1	±4.5	1169	±24	53,964	±1090.9	176.5	±1.2	0.5714	±0.0006	71,069	±150	216	±1	**70,999**	**±150**
JFYK2–14	139	11,725.6	±24.4	1092	±30	101,090	±2797.8	164.3	±1.9	0.5710	±0.0015	72,124	±314	201	±2	**72,056**	**±314**
JFYK2–15	149	7951.1	±7.2	2677	±54	28,468	±572.3	166.6	±1.4	0.5814	±0.0007	73,728	±181	205	±2	**73,654**	**±182**
JFYK2–16	156	5943.7	±5.8	327	±7	175,389	±3835.8	169.2	±1.7	0.5853	±0.0008	74,183	±212	209	±2	**74,116**	**±212**
JFYK2–17	173	9297.7	±36.9	503	±14	178,450	±5114.7	150.3	±3.7	0.5850	±0.0024	76,000	±589	186	±5	**75,934**	**±589**
JFYK2–18	180	11,027.8	±19.9	560	±11	189,648	±3862.3	146.1	±1.6	0.5844	±0.0012	76,317	±267	181	±2	**76,249**	**±267**
JFYK2–19	185	10,843.9	±11.4	590	±14	177,799	±4288.2	146.1	±1.3	0.5863	±0.0008	76,680	±198	181	±2	**76,612**	**±198**
JFYK2–20	190	12,389.2	±10.4	228	±11	526,102	±25,772.9	144.4	±0.9	0.5875	±0.0007	77,072	±167	179	±1	**77,005**	**±167**
JFYK2–21	215	13,548.7	±27.9	1368	±40	96,192	±2803.3	144.1	±1.7	0.5893	±0.0016	77,439	±350	179	±2	**77,371**	**±350**
JFYK2–22	230	12,578.9	±16.3	347	±11	353,735	±11,063.1	136.4	±1.6	0.5925	±0.0009	78,875	±249	170	±2	**78,807**	**±249**
JFYK2–23	240	12,518.9	±13.9	201	±10	600,659	±29,773.0	118.0	±1.3	0.5835	±0.0009	79,161	±222	148	±2	**79,094**	**±222**
JFYK2–24	280	9404.9	±9.6	198	±8	475,285	±19,516.8	145.1	±1.3	0.6061	±0.0009	80,540	±222	182	±2	**80,472**	**±222**
JFYK2–25	285	9221.6	±7.2	288	±11	320,392	±11,759.8	146.5	±0.9	0.6072	±0.0008	80,581	±179	184	±1	**80,513**	**±179**
JFYK2–26	290	9263.0	±9.0	201	±10	458,022	±21,685.8	136.7	±1.3	0.6031	±0.0008	80,906	±214	172	±2	**80,839**	**±214**
JFYK2–27	302	13,353.6	±30.0	1408	±41	95,331	±2774.1	139.3	±2.0	0.6097	±0.0018	81,896	±423	176	±3	**81,828**	**±423**
JFYK2–28	326	7434.5	±16.3	778	±27	97,561	±3364.3	143.1	±2.4	0.6192	±0.0017	83,334	±443	181	±3	**83,266**	**±443**
JFYK2–29	330	5535.8	±5.0	912	±20	63,060	±1364.1	154.2	±1.3	0.6304	±0.0009	84,246	±228	196	±2	**84,175**	**±228**
JFYK2–30	340	9666.4	±9.9	361	±11	275,243	±8056.7	123.0	±1.3	0.6240	±0.0009	86,766	±244	157	±2	**86,698**	**±244**
JFYK2–31	350	15,005.4	±13.9	193	±9	791,085	±36,178.7	108.9	±1.0	0.6172	±0.0008	87,154	±214	139	±1	**87,087**	**±214**
JFYK2–32	355	14,496.8	±16.2	149	±11	994,238	±70,128.2	111.1	±1.3	0.6195	±0.0009	87,355	±257	142	±2	**87,287**	**±257**
JFYK2–33	382	5125.5	±3.4	2181	±44	24,433	±491.1	106.7	±1.3	0.6305	±0.0006	90,341	±226	138	±2	**90,264**	**±226**
JFYK2–34	392	7498.9	±22.9	1250	±26	60,626	±1267.5	65.4	±2.7	0.6129	±0.0021	92,294	±633	85	±4	**92,226**	**±633**
JFYK2–35	410	10,162.5	±9.0	1262	±25	81,987	±1654.5	56.9	±1.4	0.6174	±0.0007	94,667	±270	74	±2	**94,598**	**±270**
JFYK2–36	427	15,885.7	±43.2	559	±20	293,937	±10,723.7	67.8	±2.1	0.6276	±0.0019	95,412	±561	89	±3	**95,346**	**±561**

Decay constants: λ_{230} = 9.1705 × $10^{-6}a^{-1}$; λ_{234} = 2.82206 × $10^{-6}a^{-1}$; λ_{238} = 1.55125 × $10^{-10}a^{-1}$;
* $\delta^{234}U = ([^{234}U/^{238}U]_{activity}-1) \times 1000$. $\delta^{234}U_{initial}$ was calculated based on ^{230}Th ages. **$\delta^{234}U_{initial} = \delta^{234}U_{measured} \times e^{\lambda 234 \times T}$. Corrected ^{230}Th ages assume the initial ^{230}Th/^{232}Th atomic ratio of 4.4 × 10^{-6} ± 2.2 × 10^{-6}. "BP" stands for "Before Present" where the "Present" is defined as the year 1950 CE.

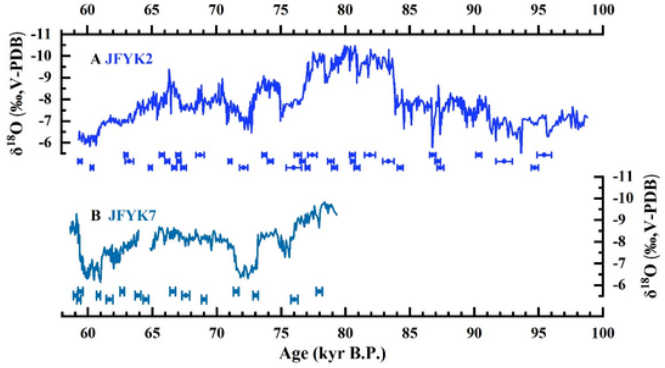

Fig. 3. $\delta^{18}O$ records of stalagmites JFYK2 (A) (this study) and JFYK7 (B) (Zhang et al., 2017); the error bars indicate the dating error (± 2σ).

soon weakening events within CIS 18 (Boch et al., 2011; Moseley et al., 2014; Moseley et al., 2020).

In the stalagmite JFYK2 $\delta^{18}O$ record, during 77.0–68.0 kyr B.P., there are two millennial-scale strong monsoon events (CIS 19 and 20), corresponding to GI 19 and GI 20. In addition, within CIS 19.1, a centennial-scale event recorded in the stalagmite JFYK2 $\delta^{18}O$ record, occurred at 68.6 kyr B.P., 500 years later than GI 19.1 (Rasmussen et al., 2014; Wolff et al., 2010). Based on a comparison of the stalagmite JFYK2 record with the NGRIP $\delta^{18}O$ record (NGRIP Members, 2004) and the European KC1 stalagmite record (Boch et al., 2011), there are obvious differences between CIS 19 and GI 19, mainly in terms of the onset and termination of CIS 19, and the duration of the shift into CIS 19 and GI 19. The onset and termination of CIS 19 (71.8 ± 0.3 and 67.0 ± 0.2 kyr B.P.) recorded by stalagmite JFYK2 are consistent with the stalagmite records from Yongxing Cave in monsoonal China (Chen et al., 2016; Zhang et al., 2017; Du et al., 2019); however, there are obvious differences in their structure. We suggest that the difference between the CIS 19 event recorded in the stalagmites of Yangkou Cave and Yongxing Cave may be related to factors such as subsample resolution, regional climate and sedimentary processes, which require further in-depth research to verify.

According to the records from stalagmites JFYK2 and JFYK7, the onset of CIS 20 was at 75.0 kyr B.P., which is supported by the record of stalagmite YX46 from Yongxing Cave (Chen et al., 2016). The European stalagmite SCH-6 record (Moseley et al., 2020) indicates that the onset of GI 20 was at 75.8 kyr B.P., ~1 kyr earlier than the onset recorded in stalagmites from the Asian monsoon region, and ~ 0.7 kyr later than the onset recorded in the NGRIP $\delta^{18}O$ record. That can possibly be attributed to age error, or to a difference in regional climate and its driving mechanisms (Moseley et al., 2020).

Comparison of the JFYK2 $\delta^{18}O$ record and Greenland ice core records indicates that the CIS events were decoupled from the GI

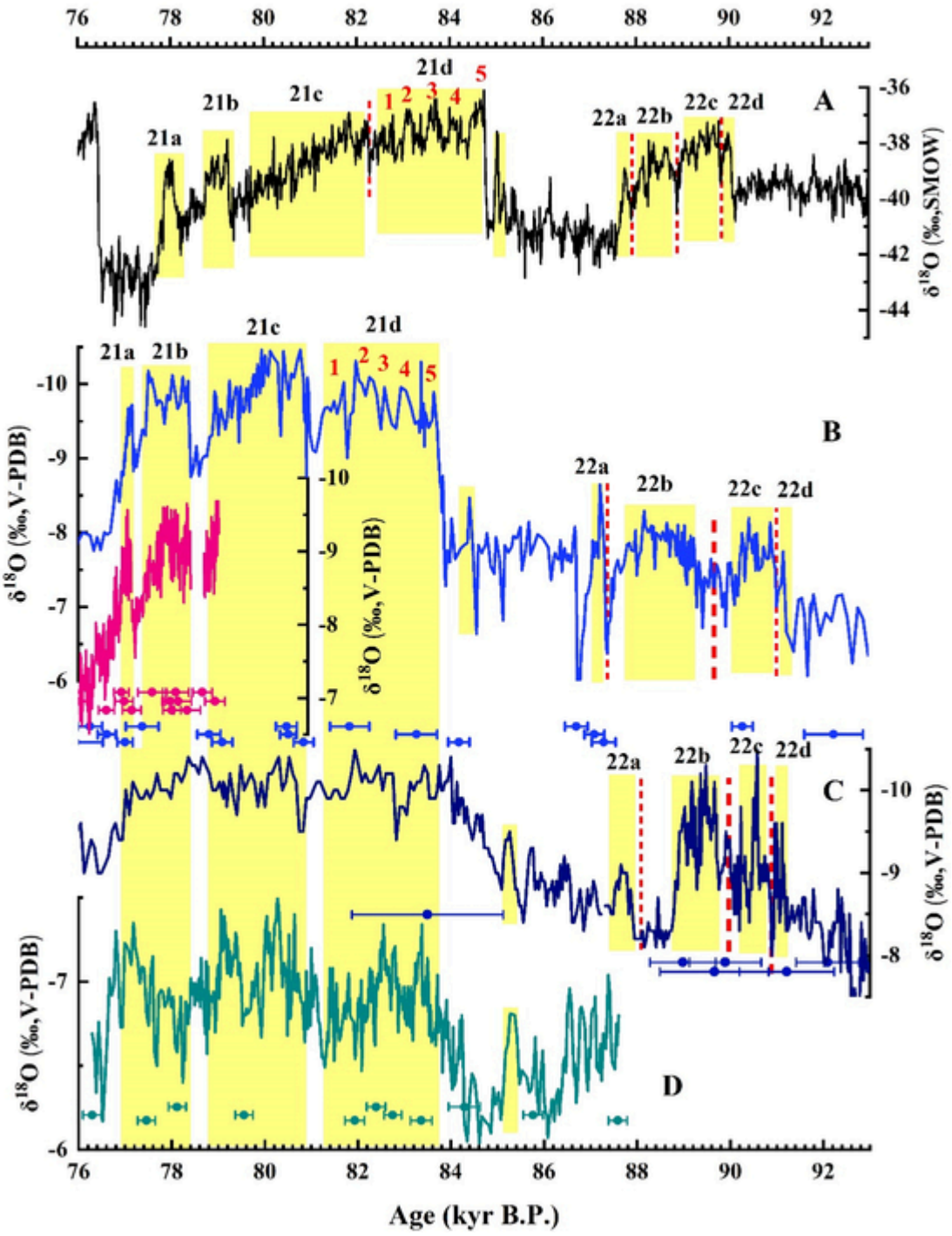

Fig. 4. Comparison of the climatic record of stalagmite JFYK2 with climatic records from Greenland and Asia. A. NGRIP ice core $\delta^{18}O$ record (NGRIP Members, 2004) (NGRIP record is plotted on the GICC05modelext timescale (Wolff et al., 2010); B. Stalagmite JFYK2 $\delta^{18}O$ record (blue) from Yangkou Cave (this study); stalagmite SX10 $\delta^{18}O$ record (pink) from Sanxing Cave (Jiang et al., 2018); C. Stalagmite PS1 $\delta^{18}O$ record from Zhenzhu Cave (Li et al., 2020); D. Stalagmite XY12 $\delta^{18}O$ record from Xianyun Cave (Zhang et al., 2020). The yellow bands represent centennial-scale abrupt climatic events, the red dotted lines represent cold events or weak monsoonal events, and the error bars indicate the dating error ($\pm 2\sigma$). (For interpretation of the references to colour in this figure legend, the reader is referred to the web version of this article.)

events, mainly in terms of the onset and termination times of millennial-scale events and in their internal structure.

4.4. Mechanisms of centennial- and millennial-scale ASM events

The stalagmite $\delta^{18}O$ records from Hulu and Sanbao caves indicate a teleconnection between Asian monsoonal and Greenland temperature changes on the millennial-scale (Wang et al., 2001, 2008; NGRIP Members, 2004). In addition, the stalagmite JFYK2 $\delta^{18}O$ records from Yangkou Cave show that the teleconnection differs substantially between glacial and interglacial periods (NGRIP Members, 2004). Based on marine records in the North Atlantic (Böhm et al., 2014) and stalagmite records from the Asian and South American (Cheng et al., 2013b; Mosblech et al., 2012), there were pronounced centennial- to millen-

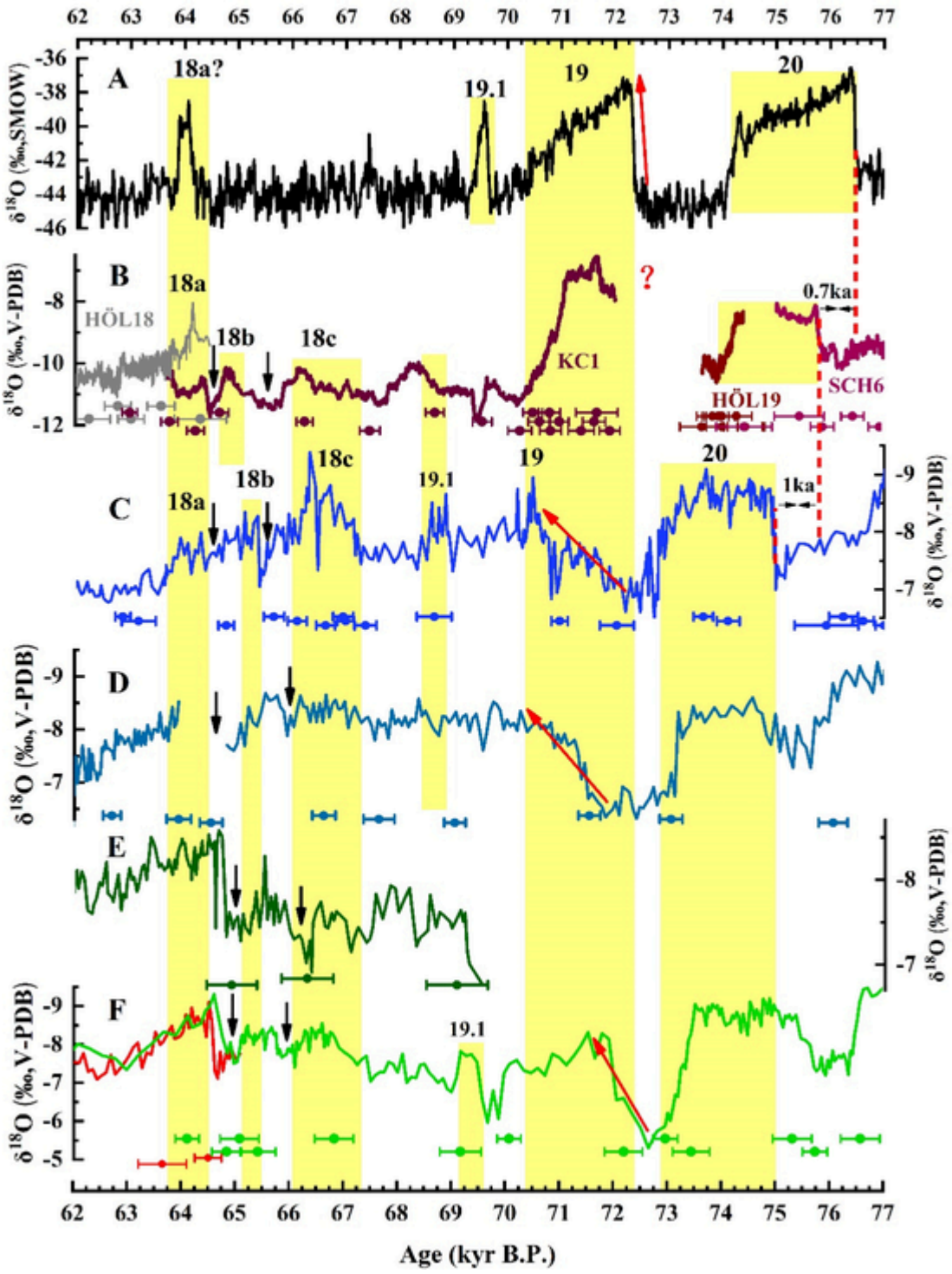

Fig. 5. Comparison of the stalagmite JFYK2 climatic record with climatic records from elsewhere. A. NGRIP ice core $\delta^{18}O$ record (NGRIP Members, 2004); B. NALPS $\delta^{18}O$ records from European Alpine Caves (Boch et al., 2011; Moseley et al., 2014; Moseley et al., 2020); C. Stalagmite JFYK2 $\delta^{18}O$ record (this study); D. Stalagmite JFYK7 $\delta^{18}O$ record (Zhang et al., 2017); E. Stalagmite XY2 $\delta^{18}O$ record from Xinya Cave (Li et al., 2007); F. Stalagmite YX46 (green) and YX55 (red) $\delta^{18}O$ records from Yongxing Cave (Chen et al., 2016). The yellow bands represent centennial- and millennial-scale abrupt climatic events. The black arrows represent cold events or weak monsoonal events, the red arrows indicate the trajectory of the shifts into GI 19 and CIS 19, and the red dotted lines indicate the onsets of GI 20 and CIS 20. (For interpretation of the references to colour in this figure legend, the reader is referred to the web version of this article.)

nial-scale abrupt climatic events within the GI 21 and GI 22 events, corresponding to the events recorded in the NGRIP $\delta^{18}O$ record during MIS 5b and 5a (NGRIP Members, 2004; Rasmussen et al., 2014; Deplazes et al., 2013; Mosblech et al., 2012; Cheng et al., 2013b) (Fig. 6). It has been demonstrated that on the centennial- to millennial-scales, the Atlantic Meridional Overturning Circulation (AMOC) and Intertropical Convergence Zone (ITCZ) played key role in transmitting high-latitude climate signals to the Asian monsoon domain (Deplazes et al., 2013; Tapio et al., 2014).

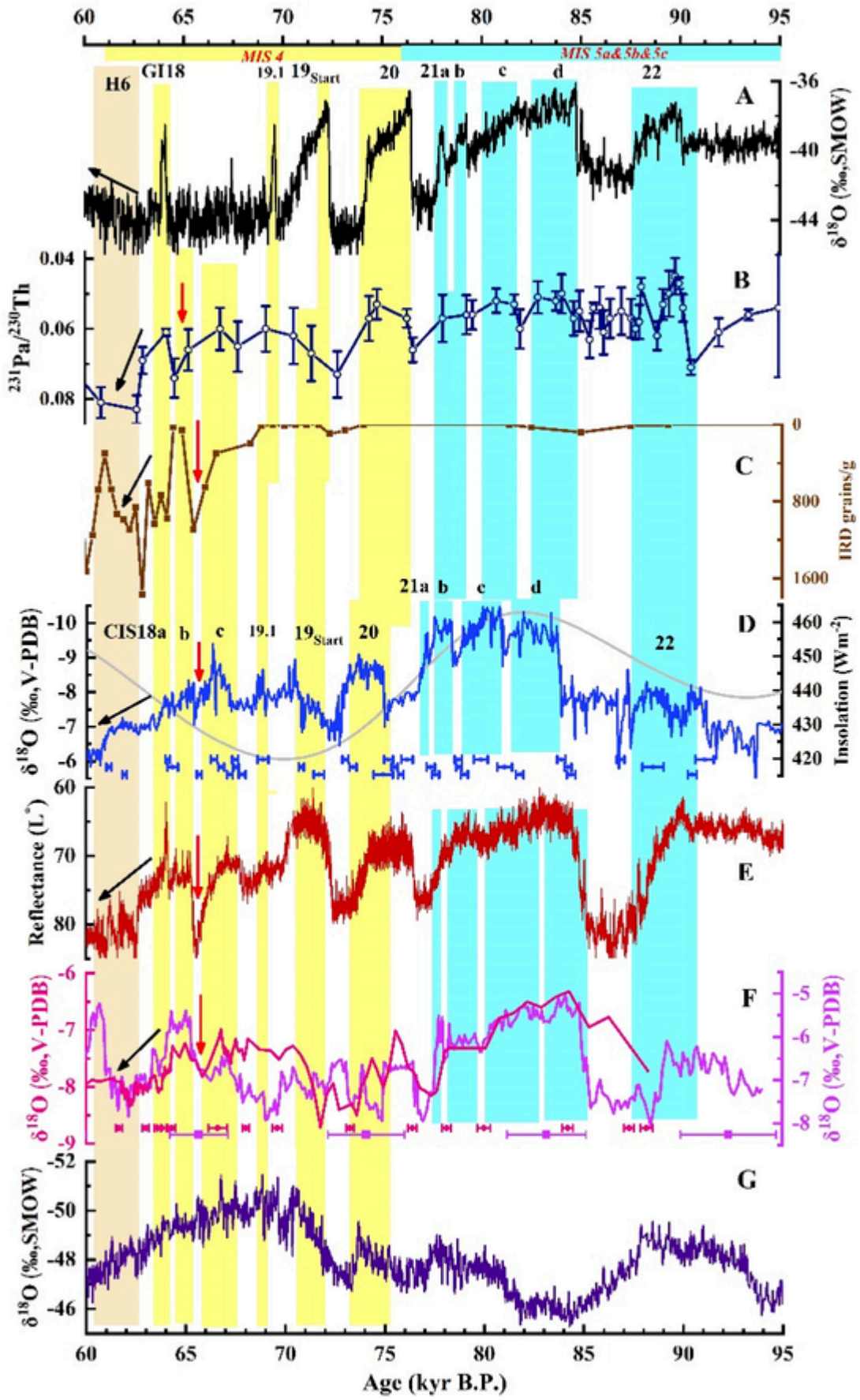
MIS 4
MIS 5a&5b&5c
H6
GI18
19.1
19Start
20
21a
b
c
d
22
A
B
C
D
E
F
G
δ18O (‰,SMOW)
231Pa/230Th
IRD grains/g
δ18O (‰,V-PDB)
Insolation (Wm-2)
Reflectance (L*)
CIS18a
Age (kyr B.P.)

Fig. 6. A. NGRIP ice core $\delta^{18}O$ record (NGRIP Members, 2004); B. Atlantic Meridional Overturning Circulation (AMOC) record reconstructed from IODP Site 1063 (Böhm et al., 2014) in the North Atlantic; C. Ice-rafted debris (IRD) record from North Atlantic core MD04–2845 (Sanchez Goñi et al., 2013); D. Stalagmite JFYK2 $\delta^{18}O$ record (this study). The gray curve shows summer (JJA) insolation at 65°N (Berger, 1978); E. Colour reflectance (L*) of Cariaco basin sediment core MD03–2621 (Deplazes et al., 2013); F. Stalagmite $\delta^{18}O$ records from South America (purple: S4 from Santiago Cave; pink: NAR-C from NAR Cave) (Mosblech et al., 2012; Cheng et al., 2013b). (G) $\delta^{18}O$ record of the EDML ice core from Antarctica (EPICA Community Members, 2006). The colored vertical bars indicate centennial- to millennial-scale events, and the black arrow indicates the trend of each paleoclimatic record during 65–60 kyr B.P. The red arrows represent cold events or weak monsoonal events. (For interpretation of the references to colour in this figure legend, the reader is referred to the web version of this article.)

During MIS 4 (Fig. 6), records of the ASM, AMOC, ITCZ and the South American summer monsoon (SASM) indicate the occurrence of similar centennial- to millennial-scale events (Mosblech et al., 2012; Cheng et al., 2013b), but they differ from those in the NGRIP $\delta^{18}O$ record (NGRIP Members, 2004). This suggests that during the MIS 5/4 transition, the relationship between the ASM and temperatures at northern high latitudes may have changed. For example, during the GI 18 event, the NGRIP $\delta^{18}O$ record only shows a short-duration temperature increase consisting of a single peak (NGRIP Members, 2004). However, records of the AMOC reveal two pronounced events of AMOC strengthening (Böhm et al., 2014), and a significant weakening event at ~65.2 kyr B.P. (Böhm et al., 2014) (Fig. 6B). In the case of the ITCZ, three pronounced northward shifts are evident (Deplazes et al., 2013), and during ~67.1–65.6 kyr B.P., there was a pronounced southward shift (Fig. 6E). In the case of the SASM, there were two pronounced weakening events (at 66.7 and 65.0 kyr B.P.) and one strengthening event (at 66.0 kyr B.P.) (Cheng et al., 2013b; Mosblech et al., 2012).

Correlation analysis of the records of the northern high-latitude temperature (NGRIP Members, 2004) and the ASM and the ITCZ (Deplazes et al., 2013) indicates a stronger relationship during MIS 5b-5a than during MIS 4, while the relationship between the ASM and ITCZ was stronger during MIS 4 (Fig. S2 D). This indicates that during the period of MIS 5b-5a, the relationship between the ASM and northern high-latitude temperature was comparatively strong, but that during MIS 4 the ASM had a close relationship with the ITCZ, and a weaker relationship with northern high-latitude temperature. This implies that the relationship between the ASM and the ITCZ and northern high-latitude temperatures may have changed during the MIS 5/4 transition, and that there was a decoupling of the ASM and high northern latitudes temperature. Notably, Sanchez Goñi et al. (2013) also observed an air–sea temperature decoupling process in Western Europe during the last interglacial–glacial transition.

The foregoing observations raise questions regarding the mechanism responsible for the change in the relationship between the Asian monsoon and high northern-latitude climate during the MIS 5/4 transition. During MIS 5, Northern Hemisphere summer insolation was high and both the sea ice cover (Hoff et al., 2016) and the continental ice cover area were low (Capron et al., 2010b; Lisiecki and Raymo, 2005). The annual average position of the ITCZ shifted northward during this period (Tapio et al., 2014) (Fig. 6E). In addition, the AMOC was relatively active and extended northward as far as the vicinity of the Nordic Seas (Guihou et al., 2011) (Fig. 6B), with a direct impact on climate change in the North Atlantic region and Greenland (Henry et al., 2016; Menviel et al., 2014). At the same time, the enhancement of the AMOC may have strengthened the impact of shifts in the ITCZ on the climate of the Asian monsoon region (Chiang and Friedman, 2012; Tapio et al., 2014). Consequently, on the centennial- to millennial-scale, there was a strong coupled relationship between the ASM and northern high latitudes.

During MIS 4, the weakening of Northern Hemisphere summer insolation led to the expansion of continental ice and sea ice cover in northern high latitudes (Kleman et al., 2013; Hoff et al., 2016), which may have led to the southward movement of the center of the ITCZ and a weakening of the AMOC (Menviel et al., 2014; Deplazes et al., 2013), in turn resulting in a weakening impact on the climate of northern high latitudes (Chiang and Friedman, 2012). Because the energy transfer from low-latitude to high-latitude regions was impeded to some extent (Jo et al., 2014), a decoupling process occurred between the Asian monsoon and the climate of high northern latitudes. The millennial-scale events during MIS 4 likely reflect this decoupling. For example, ice-rafted debris (IRD) records from the North Atlantic indicate a short-duration ice-rafting event at ~65.0 kyr B.P. (Fig. 6C), leading to a weakening of the AMOC (Böhm et al., 2014; Heinrich, 1988; Sanchez Goñi et al., 2013), which resulted in a southward shift of the ITCZ (Deplazes et al., 2013) and a weakening of the ASM (Chiang et al., 2003; Chiang and Bitz, 2005). With the subsequent recovery of the AMOC, the ITCZ returned to its previous location and the ASM was strengthened (Cheng et al., 2016; Chiang and Friedman, 2012). At the end of CIS 18, $\delta^{18}O$ in the JFYK2 stalagmite continued to be enriched, while the ASM weakened, indicating the initiation of Heinrich event 6 at 63.0 kyr B.P. In addition, there was an increase both in North Atlantic sea ice and in iceberg inputs (Hoff et al., 2016; Sanchez Goñi et al., 2013), which weakened the strength of AMOC and caused the climate to enter a 'Heinrich state', accompanied by a rapid southward shift of the ITCZ and an increase in the strength of the South American Monsoon (Cheng et al., 2013b; Cheng et al., 2012) (Fig. 6). Subsequently, based on Greenland ice core records, northern high-latitude temperatures gradually increased (Deplazes et al., 2013; Zhang et al., 2017). This indicates that during the period of maximum ice volume, during MIS 4, although the annual average position of the ITCZ moved southward, the AMOC and the ASM both weakened, and the ASM was still influenced by the ITCZ and AMOC on the centennial- to millennial-scales (Deplazes et al., 2013; Guihou et al., 2011).

Chen et al. (2016) proposed that the Asian monsoon and the climate of Antarctica have a strong coupled relationship on the suborbital timescale. The stalagmite records from Yangkou Cave show that the ASM and Antarctic temperature were closely related on the centennial timescale during MIS 4 (Fig. S3). The stalagmite JFYK2 record and the Antarctic ice core record are significantly correlated during ~76–60 kyr B.P., with correlation coefficients greater than 0.3 ($p < 0.01$, $n = 321$), indicating that the ASM was controlled by the climate of Antarctica during MIS 4. McGee et al. (2014) proposed that the decrease in temperature in Antarctica led to the strengthening of the Mascarene High, the Somali jet and northward cross-equatorial airflows, which eventually increased the intensity of the ISM and brought isotopically depleted precipitation to the Asian monsoon region (Deplazes et al., 2014; An et al., 2015; Nair et al., 2019). In addition, Wu et al. (2020) showed that the coupled relationship between the Asian summer monsoon and Antarctica mainly existed during MIS 2, and our results indicate that this relationship also existed during MIS 4. We propose that the increased influence of Antarctica may have led to the decoupling of the Asian summer monsoon from the climate of high northern latitudes during the last glacial period (Rohling et al., 2009).

5. Conclusions

We have used high-resolution (~50-year resolution) $\delta^{18}O$ measurements of a continuously growing stalagmite from Yangkou Cave in southwestern China to reconstruct the evolution of the ASM during MIS 5b to MIS 4 (~98.8–59.3 kyr B.P.). Our main conclusions are as follows:

1. During MIS 5b and 5a there were centennial-scale climatic oscillations during CIS 21 and CIS 22. These oscillations are consistent with the centennial-scale events within GI 21 and 22 in Greenland ice core records, within the dating error range, and they exhibit very similar patterns of change.
2. During MIS 4, there were three centennial-scale monsoon-strengthening events within CIS 18 (CIS 18a, 18b, and 18c), which contrast sharply with the single peak of GI 18 in the Greenland ice core record.
3. The AMOC and ITCZ are a link between the Asian monsoon and climate change in Greenland. During MIS 5, summer insolation in the Northern Hemisphere was high, and the AMOC was strengthened, and the annual average position of the ITCZ shifted northwards, which promoted a climatic teleconnection between the Asian monsoon region and northern high latitudes. However, the weakening of AMOC, the southward shift of ITCZ and the enhancement of the influence of Antarctica led to the decoupling of the ASM from the climate of northern high latitudes during MIS 4.

Declaration of Competing Interest

The authors declared that they have no conflicts of interest to this work.

Acknowledgements

We thank two anonymous reviewers for their comments that helped improve the manuscript. This work was supported by grants from the National Natural Science Foundation of China (41971109, 41572158, 41272192, 41072141 and 41972186); National Key R&D Program of China (2016YFC0502301); the Graduate Scientific Research and Innovation Foundation of Chongqing (CYS19075). Stalagmite $\delta^{18}O$ and the chronological data used to support the findings of this study are available in the supporting information file (available online). All of these data will be deposited in the World Data Center repository (https://www.ncdc.noaa.gov/data-access /paleoclimatology-data/datasets/speleothem).

Appendix A. Supplementary data

Supplementary data to this article can be found online at https://doi.org/10.1016/j.palaeo.2021.110390.

References

An, Z.S., Clemens, S.C., Shen, J., Qiang, X.K., Jin, Z.D., Sun, Y.B., Prell, W.L., Luo, J.J., Wang, S.M., Xu, H., Cai, Y.J., Zhou, W.J., Liu, X.D., Liu, W.G., Shi, Z.G., Yan, L.B., Xiao, X.Y., Chang, H., Wu, F., Ai, L., Lu, F.Y., 2011. Glacial–interglacial Indian summer monsoon dynamics. Science 333, 719–723.

An, Z.S., Wu, G.X., Li, J.P., Sun, Y.B., Liu, Y.M., Zhou, W.J., Cai, Y.J., Duan, A.M., Li, L., Mao, J.Y., Cheng, H., Shi, Z.G., Tan, L.C., Yan, H., Ao, H., Chang, H., Feng, J., 2015. Global monsoon dynamics and climate change. In: Jeanloz, R., Freeman, K.H. (Eds.), Annual Review of Earth and Planetary Sciences. pp. 29–77.

Berger, A., 1978. Long-term variations of caloric insolation resulting from the Earth's orbital elements. Quat. Res. 9, 139–167.

Boch, R., Cheng, H., Spötl, C., Edwards, R.L., Wang, X., Häuselmann, P., 2011. NALPS: a precisely dated European climate record 120–60 ka. Clim. Past 7, 1247–1259.

Böhm, E., Lippold, J., Gutjahr, M., Frank, M., Blaser, P., Antz, B., Fohlmeister, J., Frank, N., Andersen, M.B., Deininger, M., 2014. Strong and deep Atlantic meridional overturning circulation during the last glacial cycle. Nature 517, 73.

Cai, Y.J., An, Z.S., Cheng, H., Edwards, R.L., Kelly, M.J., Liu, W.G., Wang, X.F., Shen, C.-C., 2006. High-resolution absolute-dated Indian Monsoon record between 53 and 36 ka from Xiaobailong Cave, southwestern China. Geology 34, 621–624.

Cai, Y.J., Fung, I.Y., Edwards, R.L., An, Z.S., Cheng, H., Lee, J.-E., Tan, L.C., Shen, C.-C., Wang, X.F., Day, J.A., Zhou, W.J., Kelly, M.J., Chiang, J.C.H., 2015. Variability of stalagmite-inferred Indian monsoon precipitation over the past 252,000 y. Proc. Natl. Acad. Sci. 112, 201424035.

Capron, E., Landais, A., Chappellaz, J., Schilt, A., Buiron, D., Dahl-Jensen, D., Johnsen, S., Jouzel, J., Lemieux-Dudon, B., Loulergue, L., Leuenberger, M., Masson-Delmotte, V., Meyer, H., Oerter, H., Stenni, B., 2010a. Millennial and sub-millennial scale climatic variations recorded in polar ice cores over the last glacial period. Clim. Past 6, 345–365.

Capron, E., Landais, A., Lemieux-Dudon, B., Schilt, A., Masson-Delmotte, V., Buiron, D., Chappellaz, J., Dahl-Jensen, D., Johnsen, S., Leuenberger, M., Loulergue, L., Oerter, H., 2010b. Synchronising EDML and NorthGRIP ice cores using $\delta^{18}O$ of atmospheric oxygen ($\delta^{18}O_{atm}$) and CH_4 measurements over MIS5 (80–123 kyr). Quat. Sci. Rev. 29, 222–234.

Capron, E., Landais, A., Chappellaz, J., Buiron, D., Fischer, H., Johnsen, S., Jouzel, J., Leuenberger, M., Masson-Delmotte, V., Stocker, T., 2012. A global picture of the first abrupt climatic event occurring during the last glacial inception. Geophys. Res. Lett. 39, L15703.

Chen, C.J., Li, T.-Y., 2018. Geochemical characteristics of cave drip water respond to ENSO based on a 6-year monitoring work in Yangkou Cave, Southwest China. J. Hydrol. 561, 896–907.

Chen, S.T., Wang, Y.J., Cheng, H., Edwards, R.L., Wang, X.F., Kong, X.G., Liu, D.B., 2016. Strong coupling of Asian Monsoon and Antarctic climates on sub-orbital timescales. Sci. Rep. 6, 32995.

Cheng, H., Edwards, R.L., Wang, Y.J., Kong, X.G., Ming, Y.F., Kelly, M.J., Wang, X.F., Gallup, C., Liu, W.G., 2006. A penultimate glacial monsoon record from Hulu Cave and two-phase glacial terminations. Geology 34, 217–220.

Cheng, H., Fleitmann, D., Edwards, R.L., Wang, X.F., Cruz, F.W., Auler, A.S., Mangini, A., Wang, Y.J., Kong, X.G., Burns, S.J., Matter, A., 2009. Timing and structure of the 8.2 kyr BP event inferred from $\delta^{18}O$ records of stalagmites from China, Oman, and Brazil. Geology 37 (11), 1007–1010.

Cheng, H., Sinha, A., Wang, X.F., Cruz, F., Edwards, R.L., 2012. The Global Paleomonsoon as seen through speleothem records from Asia and the Americas. Clim. Dyn. 39, 1045–1062.

Cheng, H., Edwards, R., Shen, C.-C., Polyak, V., Asmerom, Y., Woodhead, J., Hellstrom, J., Wang, Y.J., Kong, X.G., Spötl, C., Wang, X.F., Alexander, Jr., E., 2013a. Improvements in ^{230}Th dating, ^{230}Th and ^{234}U half-life values, and U–Th isotopic measurements by multi-collector inductively coupled plasma mass spectrometry. Earth Planet. Sci. Lett. 371–372, 82–91.

Cheng, H., Sinha, A., Cruz, F.W., Wang, X., Edwards, R.L., d'Horta, M., Ribas, C.C., Vuille, M., Stott, L.D., Auler, A.S., 2013b. Climate change patterns in Amazonia and biodiversity. Nat. Commun. 4, 1411.

Cheng, H., Edwards, R.L., Sinha, A., Spötl, C., Yi, L., Chen, S.T., Kelly, M., Kathayat, G., Wang, X.F., Li, X.L., Kong, X.G., Wang, Y.J., Ning, Y.F., Zhang, H.W., 2016. The Asian monsoon over the past 640,000 years and ice age terminations. Nature 534, 640–646.

Cheng, H., Zhang, H., Zhao, J., et al., 2019. Chinese stalagmite paleoclimate researches: a review and perspective. Sci. China Earth Sci. 1–25.

Chiang, J.C.H., Bitz, C.M., 2005. Influence of high latitude ice cover on the marine Intertropical Convergence Zone. Clim. Dyn. 25, 477–496.

Chiang, J.C.H., Friedman, A., 2012. Extratropical cooling, interhemispheric thermal gradients, and tropical climate change. Annu. Rev. Earth Planet. Sci. 40, 383–412.

Chiang, J.C.H., Biasutti, M., Battisti, D., 2003. Sensitivity of the Atlantic Intertropical Convergence Zone to last Glacial Maximum boundary conditions. Paleoceanography 18 (18–11).

Clemens, S., Prell, W., Sun, Y.B., 2010. Orbital-scale timing and mechanisms driving late Pleistocene Indo-Asian summer monsoons: reinterpreting cave speleothem $\delta^{18}O$. Paleoceanography 25.

Dansgaard, W., Johnsen, S.J., Clausen, H.B., Dahl-Jensen, D., Gundestrup, N.S., Hammer, C.U., Hvidberg, C.S., Steffensen, J.P., Sveinbjörnsdottir, A.E., Jouzel, J., Bond, G., 1993. Evidence for general instability of past climate from a 250-kyr ice-core record. Nature 364, 218–220.

Deplazes, G., Lückge, A., Peterson, L.C., Timmermann, A., Hamann, Y., Hughen, K.A., Röhl, U., Laj, C., Cane, M.A., Sigman, D.M., 2013. Links between tropical rainfall and North Atlantic climate during the last glacial period. Nat. Geosci. 6, 213–217.

Deplazes, G., Lückge, A., Stuut, J.-B.W., Pätzold, J., Kuhlmann, H., Husson, D., Fant, M., Haug, G.H., 2014. Weakening and strengthening of the Indian monsoon during Heinrich events and Dansgaard-Oeschger oscillations. Paleoceanography 29, 99–114.

Dong, J.G., Shen, C.-C., Kong, X.G., Wang, H.-C., Jiang, X.Y., 2015. Reconciliation of hydroclimate sequences from the Chinese loess plateau and low-latitude East Asian summer monsoon regions over the past 14,500 years. Palaeogeogr. Palaeoclimatol. Palaeoecol. 435 (3), 127–135.

Dorale, J., Liu, Z., 2009. Limitations of Hendy Test criteria in judging the paleoclimatic suitability of speleothems and the need for replication. J. Cave Karst. Stud. 71, 73–138.

Du, W.J., Cheng, H., Xu, Y., Yang, X.L., Zhang, P.Z., Sha, L.J., Li, H.Y., Zhu, X.Y., Zhang, M.L., Stríkis, N.M., Cruz, F.W., Edwards, R.L., Zhang, H.W., Ning, Y.F., 2019. Timing and structure of the weak Asian Monsoon event about 73,000 years ago. Quat. Geochronol. 53, 101003.

EPICA Community Members, 2006. One-to-one coupling of glacial climate variability in Greenland and Antarctica. Nature 444, 195–198.

Guihou, A., Pichat, S., Govin, A., Nave, S., Michel, E., Duplessy, J.-C., Telouk, P., Labeyrie, L., 2011. Enhanced Atlantic meridional overturning circulation supports the last Glacial Inception. Quat. Sci. Rev. 30, 1576–1582.

Han, L.-Y., Li, T.-Y., Cheng, H., Edwards, R.L., Shen, C.-C., Li, H.-C., Huang, C.-X., Li, J.-Y., Yuan, N., Wang, H.-B., Zhang, T.-T., Zhao, X., 2016. Potential influence of tem-perature changes in the Southern Hemisphere on the evolution of the Asian summer monsoon during the last glacial period. Quat. Int. 392,

239–250.
Heinrich, H., 1988. Origin and consequences of cyclic ice rafting in the Northeast Atlantic Ocean during the past 130,000 years. Quat. Res. 29, 142–152.
Hendy, C.H., 1971. The isotopic geochemistry of speleothems—I. The calculation of the effects of different modes of formation on the isotopic composition of speleothems and their applicability as palaeoclimatic indicators. Geochem. Cosmochim. Acta 35, 801–824.
Henry, L.G., Mcmanus, J.F., Curry, W.B., Roberts, N.L., Piotrowski, A.M., Keigwin, L.D., 2016. North Atlantic Ocean circulation and abrupt climate change during the last glaciation. Science 353, 470–474.
Hercman, H., Pawlak, J., 2012. MOD-AGE: an age-depth model construction algorithm. Quat. Geochronol. 12, 1–10.
Hoff, U., Rasmussen, T.L., Stein, R., Ezat, M.M., Fahl, K.J.N.C., 2016. Sea ice and millennial-scale climate variability in the Nordic seas 90 kyr ago to present. Nat. Commun. 7, 12247.
Jiang, X.Y., He, Y.Q., Wang, X.Y., Dong, J.G., Li, Z.Z., Lone, M.A., Shen, C.-C., 2019. Sub-decadally-resolved Asian monsoon dynamics during Chinese interstadial 21 in response to northern high-latitude climate. J. Asian Earth Sci. 172, 243–248.
Jo, K., Woo, K.S., Yi, S., Yang, D.Y., Lim, H.S., Wang, Y., Cheng, H., Edwards, R.L., 2014. Midlatitude interhemispheric hydrologic seesaw over the past 550, 000 years. Nature..
Kathayat, G., Cheng, H., Sinha, A., Spötl, C., Edwards, R.L., Zhang, H.W., Li, X.L., Yi, L., Ning, Y.F., Cai, Y.J., Lui, W.L., Breitenbach, S.F.M., 2016. Indian monsoon variability on millennial-orbital timescales. Sci. Rep. 6, 24374.
Kleman, J., Fastook, J., Ebert, K., Nilsson, J., Caballero, R., 2013. Pre-LGM Northern Hemisphere ice sheet topography. Clim. Past 9, 2365–2378.
Li, T.Y., Yuan, D.X., Li, H.C., Yang, Y., Wang, J.L., Wang, X.Y., Li, J.Y., Qin, J.M., Zhang, M.L., Lin, Y.S., 2007. High-resolution climate variability of Southwest China during 57–70 ka reflected in a stalagmite $\delta^{18}O$ record from Xinya Cave. Sci. China Ser. D. 50, 1202–1208.
Li, Y.X., Rao, Z.G., Xu, Q.H., Zhang, S.R., Liu, X.K., Wang, Z.L., Cheng, H., Edwards, R.L., Chen, F.H., 2020. Inter-relationship and environmental significance of stalagmite $\delta^{13}C$ and $\delta^{18}O$ records from Zhenzhu Cave, North China, over the last 130 ka. Earth Planet. Sci. Lett. 536, 116149.
Lisiecki, L.E., Raymo, M.E., 2005. A Pliocene-Pleistocene stack of 57 globally distributed benthic $\delta^{18}O$ records. Paleoceanography 20, 522–533.
Liu, D.B., Liu, S.S., Fang, Y.F., 2019. A southern and northern control on speleothem-based Asian summer monsoon variability during MIS 4. Quat. Res. 85, 333–346.
Liu, D.B., Wang, Y.J., Cheng, H., Edwards, R.L., Kong, X.G., Wang, X., Hardt, B., Wu, J.Y., Chen, S.T., Jiang, X.Y., He, Y.Q., Dong, J.G., Zhao, K., 2010. Sub-millennial variability of Asian monsoon intensity during the early MIS 3 and its analogue to the ice age terminations. Quat. Sci. Rev. 29, 1107–1115.
Maher, B., Thompson, R., 2012. Oxygen isotopes from Chinese caves: records not of monsoon rainfall but of circulation regime. J. Quat. Sci. 27.
McGee, D., Donohoe, A., Marshall, J., Ferreira, D., 2014. Changes in ITCZ location and cross-equatorial heat transport at the last Glacial Maximum, Heinrich Stadial 1, and the mid-Holocene. Earth Planet. Sci. Lett. 390, 69–79.
Menviel, L., Timmermann, A., Friedrich, T., England, M., 2014. Hindcasting the continuum of Dansgaard-Oeschger variability: mechanisms, patterns and timing. Clim. Past 10, 63–77.
Mosblech, N.A.S., Bush, M.B., Gosling, W.D., Hodell, D., Thomas, L., Calsteren, P.V., Correametrio, A., Valencia, B.G., Curtis, J., Woesik, R.V., 2012. North Atlantic forcing of Amazonian precipitation during the last ice age. Nat. Geosci. 5, 817–820.
Moseley, G., Spötl, C., Svensson, A., Cheng, H., Brandstätter, S., Edwards, R., 2014. Multi-speleothem record reveals tightly coupled climate between Central Europe and Greenland during Marine Isotope Stage 3. Geology 42, 1043–1046.
Moseley, G.E., Spötl, C., Brandstätter, S., Erhardt, T., Luetscher, M., Edwards, R.L., 2020. NALPS19: sub-orbital-scale climate variability recorded in northern Alpine speleothems during the last glacial period. Clim. Past 16, 29–50.
Nair, A., Mohan, R., Crosta, X., Manoj, M.C., Thamban, M., Marieu, V., 2019. Southern Ocean sea ice and frontal changes during the late Quaternary and their linkages to Asian summer monsoon. Quat. Sci. Rev. 213, 93–104.
North Greenland Ice Core Project Members, 2004. High-resolution record of Northern Hemisphere climate extending into the last interglacial period. Nature 431, 147–151.
Piotrowski, A.M., Goldstein, S.L., Hemming, S.R., Fairbanks, R.G., 2005. Temporal relationships of carbon cycling and ocean circulation at glacial boundaries. Science 307, 1933–1938.
Rasmussen, S., Bigler, M., Blockley, S., Blunier, T., Buchardt, S.L., Clausen, H., Cvijanovic, I., Dahl-Jensen, D., Johnsen, S., Fischer, H., Gkinis, V., Guillevic, M., Hoek, W.Z., Lowe, J., Pedro, J., Popp, T., Seierstad, I., Steffensen, J., Svensson, A., Winstrup, M., 2014. A stratigraphic framework for abrupt climatic changes during the last Glacial period based on three synchronized Greenland ice-core records: refining and extending the INTIMATE event stratigraphy. Quat. Sci. Rev. 106, 14–28.
Rohling, E.J., Liu, Q., Roberts, A.P., Stanford, J.D., Rasmussen, S.O., Langen, P.L., Siddall, M., 2009. Controls on the East Asian monsoon during the last glacial cycle, based on comparison between Hulu cave and polar ice-core records. Quat. Sci. Rev. 28 (27–28), 3291–3302.
Sanchez Goñi, M.F., Bard, E., Landais, A., Rossignol, L., d'Errico, F., 2013. Air-sea temperature decoupling in western Europe during the last interglacial-glacial transition. Nat. Geosci. 6, 837–841.
Tan, M., 2014. Circulation effect: response of precipitation $\delta^{18}O$ to the ENSO cycle in monsoon regions of China. Clim. Dyn. 42, 1067–1077.
Tapio, S., Tobias, B., Haug, G.H., 2014. Migrations and dynamics of the intertropical convergence zone. Nature 513, 45–53.
Thornalley, D.J.R., Barker, S., Becker, J., Hall, I.R., Knorr, G., 2013. Abrupt changes in deep Atlantic circulation during the transition to full glacial conditions. Paleoceanography 28, 253–262.
Wang, Y.J., Cheng, H., Edwards, R.L., An, Z.S., Wu, J.Y., Shen, C.C., Dorale, J.A., 2001. A high-resolution absolute-dated late Pleistocene Monsoon record from Hulu Cave, China. Science 294, 2345–2348.
Wang, Y.J., Cheng, H., Edwards, R.L., Kong, X.G., Shao, X.H., Chen, S.T., Wu, J.Y., Jiang, X.Y., Wang, X.F., An, Z.S., 2008. Millennial- and orbital-scale changes in the East Asian monsoon over the past 224,000 years. Nature 451, 1090–1093.
Wang, P.X., Wang, B., Cheng, H., Fasullo, J., Guo, Z.T., Kiefer, T., Liu, Z., 2017. The global monsoon across time scales: mechanisms and outstanding issues. Earth Sci. Rev. 174.
Wolff, E.W., Chappellaz, J., Blunier, T., Rasmussen, S., Svensson, A., 2010. Millennial-scale variability during the last glacial: the ice core record. Quat. Sci. Rev. 29.
Wu, Y., Li, T.-Y., Yu, T.-L., Shen, C.-C., Chen, C.-J., Zhang, J., Li, J.-Y., Wang, T., Huang, R., Xiao, S.-Y., 2020. Variation of the Asian summer monsoon since the last glacial-interglacial recorded in a stalagmite from Southwest China. Quat. Sci. Rev. 234, 106261.
Yang, X.L., Yang, H., Wang, B.Y., Huang, L.J., Shen, C.-C., Edwards, R.L., Cheng, H., 2019a. Early-Holocene monsoon instability and climatic optimum recorded by Chinese stalagmites. Holocene 29 (6), 1059–1067.
Yang, Y., Yang, R.W., Cao, J., Zhao, J.Y., Cheng, H., Wang, J., 2019b. Relationship between the Asian summer monsoon circulation and speleothem $\delta^{18}O$ of Xiaobailong Cave. Clim. Dyn. 53, 6351–6362.
Yuan, D.X., Cheng, H., Edwards, R.L., Dykoski, C.A., Kelly, M.J., Zhang, M.L., Qing, J.M., Lin, Y.S., Wang, Y.J., Wu, J.Y., 2004. Timing, duration, and transitions of the last interglacial Asian monsoon. Science 304, 575–578.
Zhang, P.Z., Cheng, H., Edwards, R.L., Chen, F.H., Wang, Y.J., Yang, X.L., Liu, J., Tan, M., Wang, X.F., Liu, J.H., An, C.L., Dai, Z.B., Zhou, J., Zhang, D.Z., Jia, J.H., Jin, L.Y., Johnson, K.R., 2008. A test of climate, sun, and culture relationships from an 1810-year Chinese cave record. Science 322, 940–942.
Zhang, T.-T., Li, T.-Y., Cheng, H., Edwards, R.L., Shen, C.-C., Spötl, C., Li, H.-C., Han, L.-Y., Li, J.-Y., Huang, C.-X., Zhao, X., 2017. Stalagmite-inferred centennial variability of the Asian summer monsoon in Southwest China between 58 and 79 ka B.P. Quat. Sci. Rev. 160, 1–12.
Zhang, H.W., Ait Brahim, Y., Li, H.Y., Zhao, J.Y., Kathayat, G., Tian, Y., Baker, J., Wang, J., Zhang, F., Ning, Y.F., Edwards, R.L., Cheng, H., 2019a. The Asian summer monsoon: teleconnections and forcing mechanisms-a review from Chinese speleothem $\delta^{18}O$ records. Quaternary 2 (3), 26.
Zhang, J.W., Liu, S.S., Liu, D.B., Kong, X.G., Fang, Y.F., 2019b. Correlation between oxygen and carbon isotopes of speleothems from Tian'e Cave, Central China: insights into the phase relationship between Asian summer and winter monsoons. J. Asian Earth Sci. 180, 103884.
Zhang, X., Xiao, H.Y., Chou, Y.-C., Cai, B.G., Lone, M.A., Shen, C.-C., Jiang, X.Y., 2020. A detailed East Asian monsoon history of Greenland Interstadial 21 in southeastern China. Palaeogeogr. Palaeoclimatol. Palaeoecol. 552, 109752.
Zhao, K., Wang, Y., Edwards, R.L., Cheng, H., Liu, D., 2010. High-resolution stalagmite δ18O records of Asian monsoon changes in central and southern China spanning the MIS 3/2 transition. Earth Planet. Sci. Lett. 298, 191–198.
Zhou, H.Y., Zhao, J.X., Feng, Y.X., Chen, Q., Mi, X.J., Shen, C.-C., He, H.B., Liang, Y., Liu, S.H., Lin, C., Huang, J.Y., Zhu, L.Y., 2014. Heinrich event 4 and Dansgaard/Oeschger events 5–10 recorded by high-resolution speleothem oxygen isotope data from Central China. Quat. Res. 82, 394–404.